Supplementary Information for: GDDRP-CMIP6: Global Daily Runoff Projections from Bias-Corrected and Downscaled CMIP6 Forcing

This document contains Supplementary Methods S1–S3 and Supplementary Figures S1–S3.

Supplementary Methods S1. Derivation of humidity and surface pressure forcing

Daily maximum and minimum temperature, precipitation, longwave and shortwave radiation, and wind speed are taken directly from the NEX-GDDP-CMIP6 members. Actual vapor pressure is derived from relative humidity and the saturation vapor pressure computed with the Tetens formula (Eqs. S1, S2; Allan et al., 1998; Murray, 1967), and surface pressure is estimated from the grid-mean elevation and actual vapor pressure using the hypsometric equation (Eqs. S3–S5).

$$e_s = \begin{cases} 0.61078\, exp\left(\frac{17.270T}{T+237.3}\right) & T \geq 0 \\ 0.61078\, exp\left(\frac{21.875T}{T+265.5}\right) & T < 0 \end{cases} \quad \text{Eq. S1}$$

$$e_a = \frac{RH}{100} e_s \quad \text{Eq. S2}$$

$$q = \frac{1000\varepsilon e_a}{p-(1-\varepsilon)1000e_a} \quad \text{Eq. S3}$$

$$T_v = (T + 273.15)(1 + 0.608q) \quad \text{Eq. S4}$$

$$p = p_0 exp(-\frac{gz}{R_2 T_v}) \quad \text{Eq. S5}$$

where, T is the daily average temperature in degrees Celsius (°C); RH is the relative humidity expressed as a percentage (%); e_s is the saturation vapor pressure (kPa); e_a is the actual vapor pressure (kPa); q is the specific humidity (kg kg^{-1}); T_v is the virtual temperature (K); p is the surface air pressure (kPa) at elevation z; p_0 is the reference sea level pressure, set to the standard value of 101.325 kPa; g is the standard gravitational acceleration, set to 9.80665 m s^{-2}. R_d is the specific gas constant for dry air, set to 287.05 J kg^{-1} K^{-1}; ε is the ratio of the molar mass of water vapor to that of dry air, set to 0.622. Equations (S3) to (S5) are mutually dependent. The system is solved iteratively. The initial estimate assumes dry air, and successive iterates are obtained by evaluating Eqs. S3 – S5 in sequence.

Supplementary Methods S2. VIC model structure and calibrated parameters

VIC is a physically based macroscale land-surface model whose core features include a spatial probability distribution characterizing the sub-grid heterogeneity of soil water storage capacity, a vegetation mosaic partitioned by land-cover type to represent sub-grid variations in evapotranspiration, a nonlinear recession relationship describing baseflow drainage from the lowest soil layer, and elevation bands accounting for topographic effects on precipitation and snow.

The sensitive parameters for calibration include the variable infiltration curve parameter (b), the thickness of the second soil layer (d2), and the fraction of the maximum baseflow rate at which the nonlinear recession begins (Ds). Each corresponds to a well-defined hydrological process: b determines the shape of the probability distribution of sub-grid soil water storage capacity and thereby controls the partitioning of precipitation between infiltration and direct surface runoff; d2 sets the storage capacity of the middle soil layer, influencing the seasonal memory of soil moisture, the water supply for evapotranspiration, and the magnitude and recession of baseflow; and Ds locates the inflection point at which the baseflow recession curve passes from its linear to its nonlinear segment, governing the timing and shape of the baseflow response. Although the optimal parameter values are affected by biases in the meteorological forcing, the hydrological simulations can still benefit from calibration against independent data sources, because it captures the relative spatial heterogeneity of soil responses.

The globally calibrated parameter fields of Lin et al. (2019) are adopted in this study. They were calibrated grid by grid using the Shuffled Complex Evolution algorithm (SCE-UA; Duan et al., 1992) against the Global Streamflow Characteristics Dataset (GSCD; Beck et al., 2015). Supplementary Figures S1 and S2 compare the discharge simulated with the default and calibrated parameters using the ACCESS-CM2 forcing. With the default parameters, discharge is severely underestimated at most stations, especially for small basins and low flows, whereas the calibrated parameters markedly improve the performance.

Supplementary Methods S3. CaMa-Flood configuration

The model discretizes the global river network into hydrological computation units termed unit-catchments, using a hybrid grid-vector river map that assigns an irregularly shaped unit-catchment to each regular grid cell, thereby achieving a physically based parameterization of sub-grid topography while retaining computational efficiency at the global scale. The river network topology and the sub-grid topographic parameters of channels and floodplains are derived from the high-resolution global hydrography dataset MERIT Hydro (Yamazaki et al., 2019); the simulations in this study use a 1-arcminute high-resolution map and perform global simulations at a 6-arcminute (approximately 0.1°) resolution. Water storage is the sole prognostic variable, and its evolution is solved from the water balance equation, which accounts for upstream inflow, downstream outflow, and lateral runoff forcing; water level and inundated areas are diagnosed from the storage of each unit-catchment in combination

with the sub-grid topographic parameters. River discharge and flow velocity are computed with the local inertial approximation of the shallow-water equations (Bates et al., 2010; Yamazaki et al., 2013), which captures backwater effects and remains numerically stable under an adaptive time step satisfying the Courant-Friedrichs-Lewy condition. To represent complex flow paths that the single-downstream assumption cannot describe, the model further incorporates a bifurcation scheme (Yamazaki et al., 2014), which automatically identifies bifurcating channels from high-resolution topography and allows one unit-catchment to distribute flow to multiple downstream units, with the bifurcated discharge likewise solved by the local inertial equation; this is particularly important for hydrodynamic simulation in deltas and other strongly bifurcated regions. Combining explicit momentum dynamics with high computational efficiency, CaMa-Flood has become a widely adopted framework for global runoff routing, flood hazard assessment, and climate-change impact studies. This study employs the recently released GPU-accelerated version, a re-implementation of the original model for graphics processing unit (GPU) architectures in which the core algorithms, including irregular river network routing, runoff interpolation, and water depth diagnosis, are recast as massively parallel operations while preserving the physics of the original model (Kang et al., 2026). Benchmark tests show that this version achieves roughly an order-of-magnitude speed-up relative to a 192-core CPU baseline, with negligible numerical differences from the reference solution.

Supplementary Figures

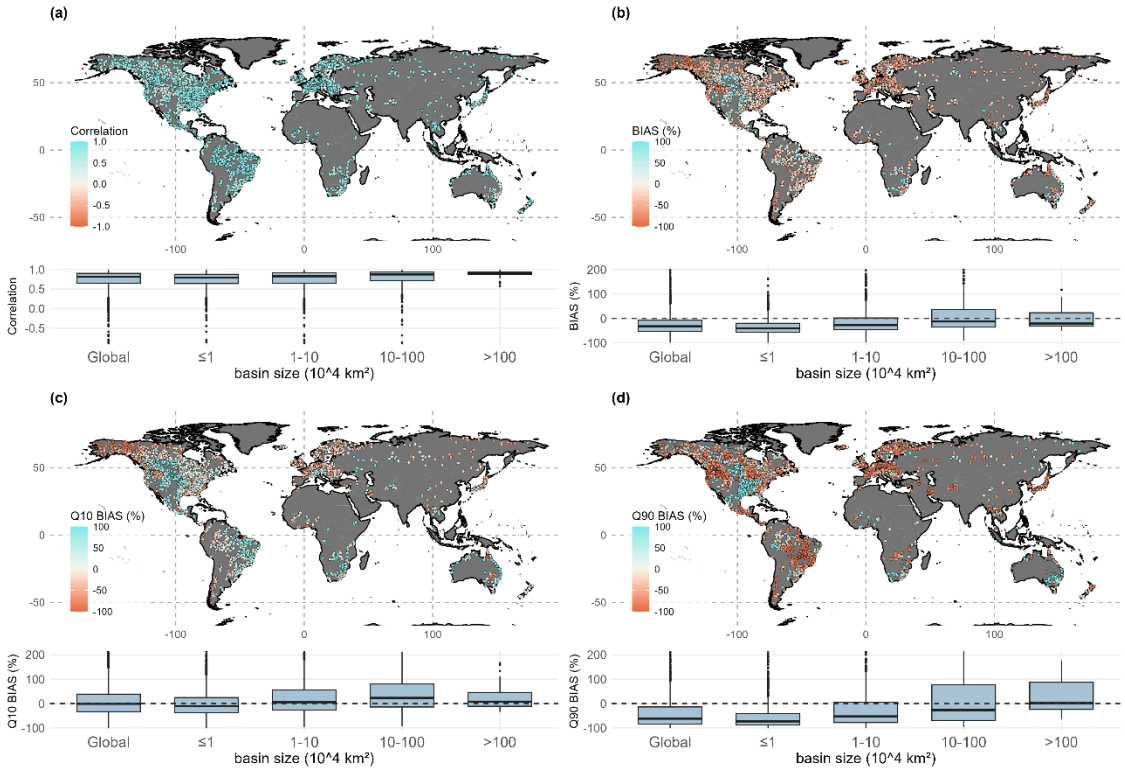

Supplementary Figure S1. Evaluation of discharge simulated with the default VIC parameters using the ACCESS-CM2 forcing against GRDC observations.

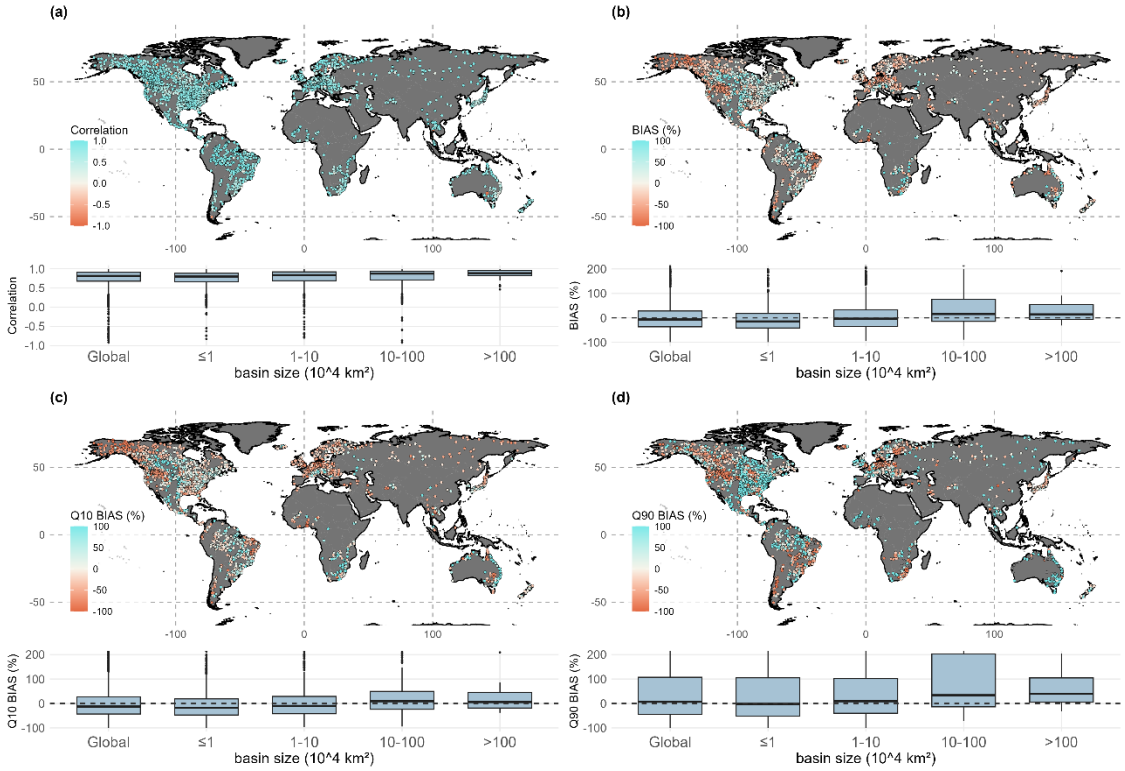

Supplementary Figure S2. As Supplementary Figure S1, but for the calibrated VIC parameters.

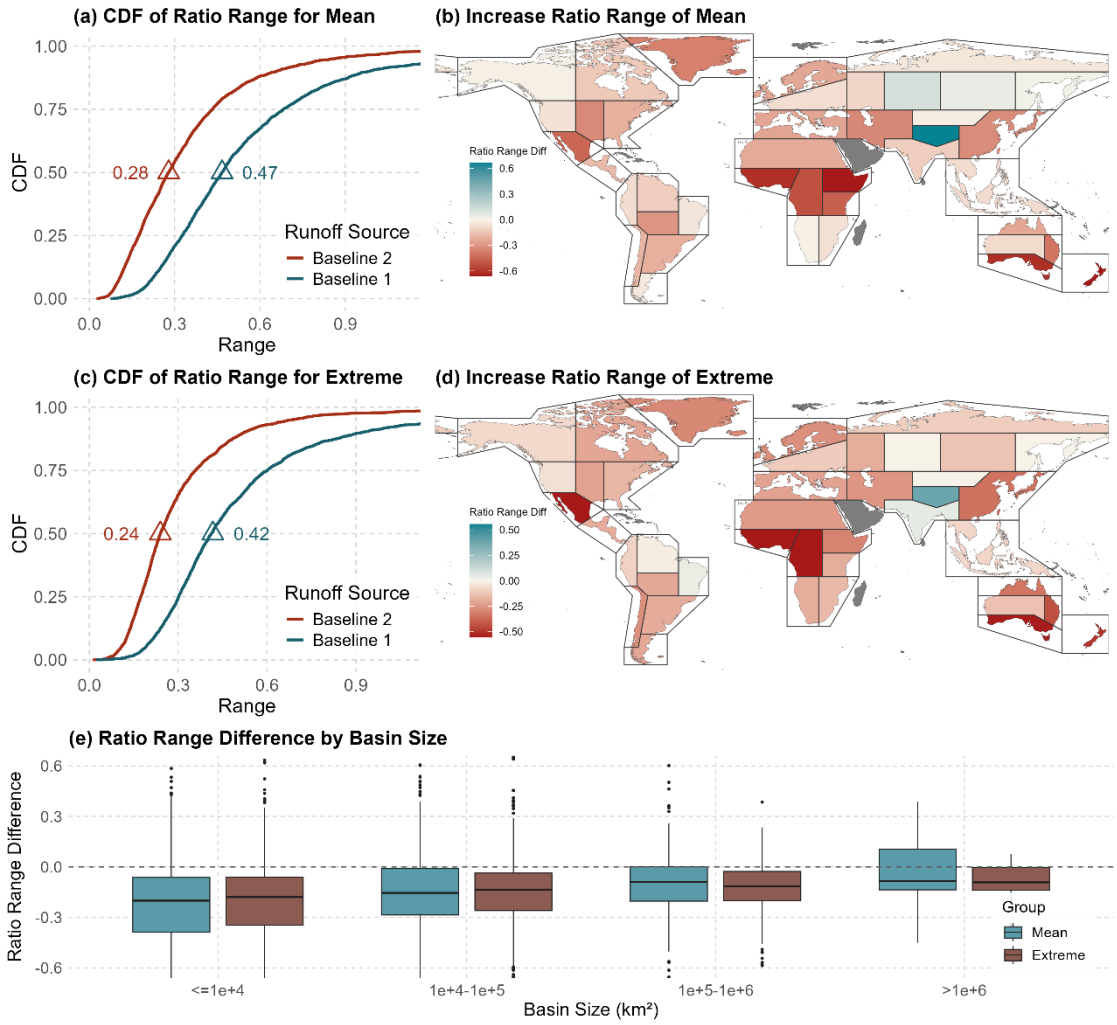

Supplementary Figure S3. Inter-member range of the projected change ratios under SSP5-8.5 for Baseline 2, for mean (a) (b) and extreme (c)(d) discharge.

Supplementary References

Allan, R., Pereira, L., Smith, M., 1998. Crop evapotranspiration-Guidelines for computing crop water requirements-FAO Irrigation and drainage paper 56.

Bates, P.D., Horritt, M.S., Fewtrell, T.J., 2010. A simple inertial formulation of the shallow water equations for efficient two-dimensional flood inundation modelling. J. Hydrol. 387, 33–45. https://doi.org/10.1016/j.jhydrol.2010.03.027

Beck, H.E., Roo, A. de, Dijk, A.I.J.M. van, 2015. Global Maps of Streamflow Characteristics Based on Observations from Several Thousand Catchments. J. Hydrometeorol. 16, 1478–1501. https://doi.org/10.1175/JHM-D-14-0155.1

Duan, Q., Sorooshian, S., Gupta, V., 1992. Effective and efficient global optimization for conceptual

rainfall-runoff models. Water Resour. Res. 28, 1015–1031. https://doi.org/10.1029/91WR02985

Kang, S., Yin, J., Yamazaki, D., 2026. CaMa-Flood-GPU: a GPU-based hydrodynamic model implementation for scalable global simulations. Geosci. Model Dev. 19, 5623–5640. https://doi.org/10.5194/gmd-19-5623-2026

Liang, X., Letternmaier, D., Wood, E., Burges, S., 1994. A simple hydrologically based model of land surface water and energy fluxes for general circulation models. J. Geophys. Res. Atmos. 99, 14415–14428. https://doi.org/10.1029/94JD00483

Lin, P., Pan, M., Beck, H.E., Yang, Y., Yamazaki, D., Frasson, R., David, C.H., Durand, M., Pavelsky, T.M., Allen, G.H., Gleason, C.J., Wood, E.F., 2019. Global Reconstruction of Naturalized River Flows at 2.94 Million Reaches. Water Resour. Res. 55, 6499–6516. https://doi.org/10.1029/2019WR025287

Murray, F.W., 1967. On the Computation of Saturation Vapor Pressure. J. Appl. Meteorol. Climatol. 6, 203–204.

Yamazaki, D., de Almeida, G.A.M., Bates, P.D., 2013. Improving computational efficiency in global river models by implementing the local inertial flow equation and a vector-based river network map. Water Resour. Res. 49, 7221–7235. https://doi.org/10.1002/wrcr.20552

Yamazaki, D., Ikeshima, D., Sosa, J., Bates, P.D., Allen, G.H., Pavelsky, T.M., 2019. MERIT Hydro: A High-Resolution Global Hydrography Map Based on Latest Topography Dataset. Water Resour. Res. 55, 5053–5073. https://doi.org/10.1029/2019WR024873

Yamazaki, D., Ikeshima, D., Tawatari, R., Yamaguchi, T., O'Loughlin, F., Neal, J.C., Sampson, C.C., Kanae, S., Bates, P.D., 2017. A high-accuracy map of global terrain elevations. Geophys. Res. Lett. 44, 5844–5853. https://doi.org/10.1002/2017GL072874

Yamazaki, D., Kanae, S., Kim, H., Oki, T., 2011. A physically based description of floodplain inundation dynamics in a global river routing model. Water Resour. Res. 47. https://doi.org/10.1029/2010WR009726

Yamazaki, D., Sato, T., Kanae, S., Hirabayashi, Y., Bates, P.D., 2014. Regional flood dynamics in a bifurcating mega delta simulated in a global river model. Geophys. Res. Lett. 41, 3127–3135. https://doi.org/10.1002/2014GL059744